IEEE Access
Multidisciplinary | Rapid Review | Open Access Journal

Received 15 March 2024, accepted 10 April 2024, date of publication 16 April 2024, date of current version 24 April 2024.

Digital Object Identifier 10.1109/ACCESS.2024.3389703

RESEARCH ARTICLE

Design, Mathematical Modeling, and Control of an Underactuated 3-DOF Experimental Helicopter

OSAMAH TALAL MAKKI[1], SEYYED SAJJAD MOOSAPOUR[1], SALEH MOBAYEN[2], (Member, IEEE), AND JAFAR HEYRANI NOBARI[3]

[1]Faculty of Engineering, Shahid Chamran University of Ahvaz, Ahvaz 6135783151, Iran
[2]Graduate School of Intelligent Data Science, National Yunlin University of Science and Technology, Douliu, Yunlin 640301, Taiwan
[3]Department of Electrical and Computer Engineering, K. N. Toosi University of Technology, Tehran 19697, Iran

Corresponding author: Seyyed Sajjad Moosapour (s.moosapour@scu.ac.ir)

This work was supported by the Shahid Chamran University of Ahvaz under Grant SCU.EE1402.278.

ABSTRACT This article covers the design, implementation, mathematical modelling, and control of a multivariable, underactuated, low-cost, three-degrees-of-freedom experimental helicopter system (namely a 3-DOF helicopter). The system is considered an essential benchmark for the development and evaluation of control algorithms and identification methods as it mimics real helicopters and UAVs. The system is multivariable and difficult to control due to its underactuation characteristics. In addition, it presents further challenges in modelling and control analysis in terms of high nonlinearity, coupling, uncertainty, and unmodeled dynamics. In this scene, the system is designed, developed, and operated virtually in SolidWorks using the necessary hardware and software. A new accurate multivariable coupled nonlinear mathematical model is derived and proposed. The model takes into account the complex dynamics and interactions between the system components, providing a more comprehensive representation of the real system compared to previous models. System parameters are then identified using the Sum of the Square Error (SSE) algorithm, and the mathematical model is compared to the practical results in many different scenarios via Simulink. Experimental tests confirmed the mathematical model and robust performance of the implemented experimental 3-DOF helicopter system, as well as the ability of the proposed controller to stabilize the helicopter and track different trajectories in the presence of uncertainties and cross-coupling effects.

INDEX TERMS Underactuated 3-DOF helicopter, nonlinear modeling, parameter identification, cross-coupling control.

I. INTRODUCTION

Drones are becoming increasingly popular because they can be used in a variety of ways, such as search and rescue, military reconnaissance, border control, agriculture, and academic research [1]. In recent years, UAVs of different sizes, structures, performances, and complexities have also been manufactured and used in numerous tasks with different scenarios [2]. In addition, technology, computers, and electrical equipment have made control theory increasingly important in UAV development to handle complicated tasks [3], [4], [5], [6], [7], [8], [9].

UAVs are underactuated systems in which the number of control signals is less than the configuration variables [10], [11]. Nowadays, underactuated systems are popular in the aviation sector, as the number of actuators needs to be reduced to decrease weight and costs. Normally, implementing controllers in the primary system and evaluating their performance for accurate movements is a challenging task [12]. Many 3-DOF laboratory helicopter platforms, such

The associate editor coordinating the review of this manuscript and approving it for publication was Wei Xu.

© 2024 The Authors. This work is licensed under a Creative Commons Attribution-NonCommercial-NoDerivatives 4.0 License.
For more information, see https://creativecommons.org/licenses/by-nc-nd/4.0/

as GoogolTech [13], LASS [14], and Quanser models [15], have been developed to imitate propeller-actuated UAVs and helicopters for better understanding. They are essential for validating flight control algorithms off-board. However, complex dynamics, uncertainty, coupling, and attitude control are the biggest challenges in these systems.

The 3-DOF helicopter system is an underactuated laboratory model that behaves like a tandem-rotor helicopter powered by two actuators. Furthermore, in addition to the uncertainty of the model parameters, the system exhibits higher-order nonlinearity, cross-coupling, actuator saturation/faults [16], and input saturation and is susceptible to external disturbances. Therefore, implementation, modelling, and control are considered challenging tasks.

Many studies have been carried out on the 3-DOF laboratory helicopter models. The focus of these studies was on the modelling and implementation of control algorithms. The classic modelling of the 3-DOF helicopter model was developed by Quanser Inc. [17]. In [18], Apkarian used MAPLE to derive a linearized mathematical model. The authors in [19] derived the nonlinear dynamics using twists and wrenches. In [20], nonlinear dynamics with coupled state variable equations for the 3-DOF helicopter were presented. Furthermore, the Lagrange equation was used to derive two simplified nonlinear models in [21].

In [22], researchers minimized the complexity of the mathematical model for the Quanser helicopter, as described in [19], by excluding terms that had a minimal impact on the total kinetic energy. In [23], an improved nonlinear model for a 3-DOF helicopter was developed that takes into account the coupling effect with friction phenomena. Additionally, a nonlinear mathematical model with some simplifications for the Quanser model was used in [24]. Chabir et al. [25] introduced a linear model using physical laws and Newton's second law. They neglected friction forces and gravitational torque. Rajappa et al. [26] considered the helicopter as a robot manipulator. They developed nonlinear dynamics using modified Denavit-Hartenberg robotic notations and estimated unknown parameters using an identification method based on the inverse dynamic model. Another mathematical model for the LAAS 3-DOF helicopter was derived based on the least-square estimator in [14].

Due to their wide range of applications, several control algorithms have been implemented and put into practice on 3-DOF helicopter models. Therefore, the control methods are generally divided into three categories, one, two, and three-channel approaches, based on the number of channels regulated. In the single-channel regulation approach, one channel is considered and controlled, whereas other channels are set free [14]. In a two-channel control approach, pitch and elevation angles were considered and controlled, whereas the travel angle was set free [27], [28], [29], [30], [31], [32].

On the other hand, the regulation of three channels means that pitch, elevation, and travel angles are under control. Three-channel control is more effective and necessary in practical engineering applications and theoretical foundations because it is identical to the existing control systems for both UAVs and helicopters. Many three-channel approaches were recorded in the literature, such as neural network [33], continuous twisting algorithm (CTA) [34], trajectory tracking with prescribed performance [35], and fault-tolerant attitude tracking [36]. Additionally, in [37], the authors proposed a self-tuned PID controller for the Quanser 3-DOF helicopter using a stable adaptation mechanism.

In fact, the 3-DOF helicopter proved to be a valuable test system for determining the robustness of control systems, as demonstrated by the research reviewed in this study. This system offers complex features that provide a unique combination of nonlinearity and controllability. In addition, the contribution of this paper is to construct a new 3-DOF experimental helicopter system for educational purposes. Whereas finding very few 3-DOF helicopter designs in the literature, particularly the Quanser model, we introduce a new design using readily available cheap spares. Based on the parts discussed in this paper, instructors and students can create their own cheap 3-DOF helicopter devices.

The primary motivation for developing this platform is to provide a more effective educational tool within control systems engineering. Traditional models are either not complex enough to effectively simulate real-world scenarios or are prohibitively expensive for many educational institutions. We aimed to fill this gap by providing a model that is both low-cost and realistic to enable the same problems that engineers face in practice. Through the inclusion of novel dynamics in this work, our platform aims to provide students and researchers with insight into and intuition about multivariable system control. This sort of hands-on experience is vital in developing the problem-solving skills that have become so important within modern control systems engineering. In addition, these novel dynamics provide a whole new range of experiments to be run. Students are able to try out a wide variety of control algorithms and can investigate how each performs within the real world, creating a far more complete learning experience and better preparing students for their careers.

Thus, through this objective, the instructors and learners can enhance the learning process for a better understanding of the modelling and identification procedures and to implement hands-on training on relevant electronic issues like sensors, actuators, building an electrical circuit as well as control systems. This paper provides a progressive set of instructions from the beginning to create a 3-DOF helicopter from scratch. Also, this study offers detailed instructions for deriving mathematical models and identification procedures for unknown parameters. Besides, comprehending the mechanics of aerodynamic forces in the existence of feedback control is an essential aspect of the control engineering curriculum, as observed in the literature. The main effect of this work is to offer teachers and scholars the possibility to acquire such information, hence optimizing the learning experience. Furthermore, this investigation examines some of the issues scholars may encounter whereas controlling aerodynamic

forces. In addition to being confirmed by practicable data, we illustrate the potential to control the suggested model helicopter utilizing a basic algorithm such as PID. The following are the main contributions of this study:

1) A 3-DOF laboratory experimental helicopter is designed and developed with a unique, low-cost structure to validate various control and identification algorithms.
2) A complete and detailed explanation of the development stages of the mechanical and electrical parts is presented.
3) A novel and considerably accurate mathematical model is developed by incorporation of previously unmodeled dynamics. These dynamics were left out of many previously published works. Therefore, considering these dynamics translates into superior performance in application areas of control and identification.
4) The unknown system parameters are determined by a known identification technique to achieve a complete and precise mathematical model. It is important to note that the identification method selected for this work allows for superior accuracy of system parameters estimation, which further results in a model that more closely resembles the actual system dynamics.
5) The correlation and validity of the mathematical model to the existing system are investigated through comparative simulations with different scenarios.

The remainder of this paper is organized as follows. Section II introduces the design process and briefly describes the mechanical and electrical components. Section III presents the mathematical model of the system. The parameter identification and comparative simulation results are provided in Section IV. Section V presents the control scheme with experimental results. Furthermore, the practical results of the control strategy are presented in Section VI. In Section VII, a brief discussion highlights the main findings and limitations of the study. Some conclusions of this paper are drawn in Section VIII.

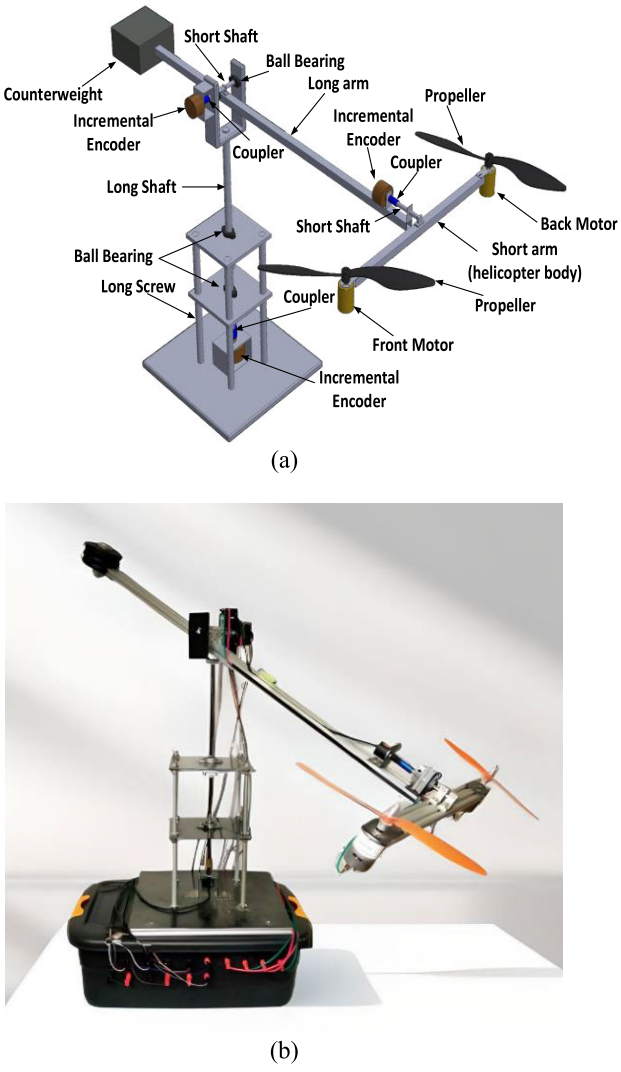

FIGURE 1. (a) Design of 3-DOF helicopter model using SolidWorks software, (b) Implemented 3-DOF helicopter model.

II. MATERIALS AND METHODS

The system is designed based on the specifications of a real tandem-rotor helicopter. A three-dimensional structure is constructed using SolidWorks software. Fig. 1(a) shows the final three-dimensional design for the proposed 3-DOF helicopter system, whereas Fig. 1(b) shows the real implemented system.

A. MECHANICAL COMPONENTS

The proposed 3-DOF helicopter has a main iron plate that forms the base of the system. Two horizontal plates are attached above the main plates with long screws. Fig. 2(a) shows the plates supporting the long shaft, travel encoder, and other components. An iron bracket holds a vertical travel encoder on the main plate. A coupling connects the encoder to a long cylindrical shaft. The long shaft positioned in the main plate passes through the centers of the other small plates through two ball bearings, Fig. 2(a). The long iron shaft supports the long arm of the helicopter by a U-shaped iron stand, as shown in Fig. 2(b). In addition, ball bearings and a small cylindrical iron shaft ensure that the long arm of the helicopter slides smoothly on the U-stand. A metal bracket secures the elevation encoder and is attached horizontally to the U-shaped stand.

In addition, a coupling attaches the encoder to the short shaft. This encoder measures the elevation angle, as shown in Fig. 2(b). A ball bearing and a short cylindrical shaft connect the long arm at one end to the short arm, which forms the body of the helicopter, and a counterweight is mounted at the other end. The counterweight is responsible for lowering the effective mass of the helicopter in order to raise it through propulsion. In addition, a coupling connects the short arm

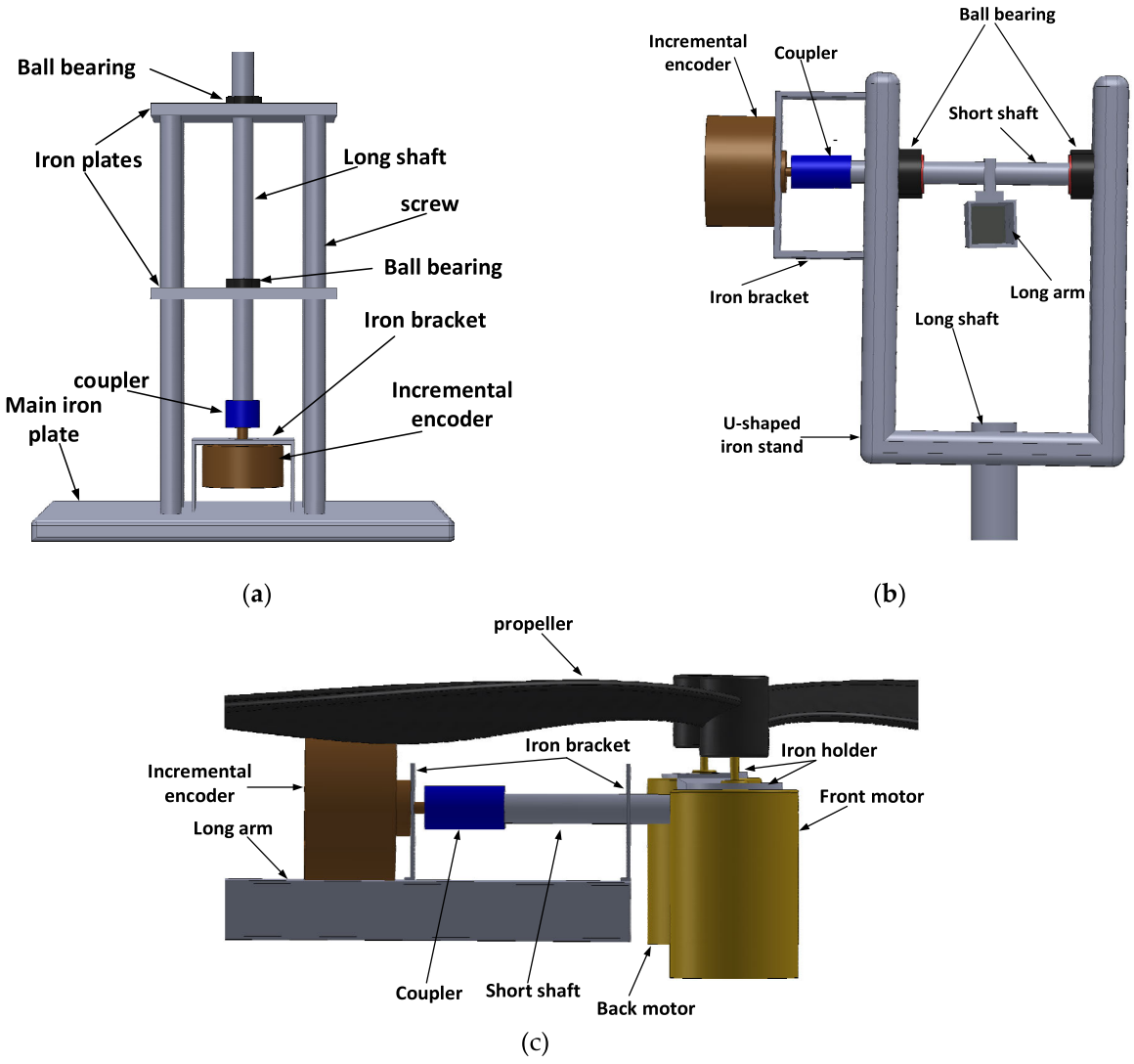

FIGURE 2. Mechanical components. (a) travel channel. (b) elevation channel (c) pitch channel.

of the helicopter to an encoder mounted on an iron bracket on the long arm and is used to measure the pitch angle, as shown in Fig. 2(c). The long and short arms can move in elevation, travel, and pitch directions. Due to mechanical limitations, the long arm can only be rotated between $+180^0$ and -180^0 around the travel axis and between $+25^0$ and -25^0 around the elevation axis. The short arm has a range of $+50^0$ to -50^0. Two motors with two propellers are attached to each end of the helicopter body (short arm) via iron holders.

B. ELECTRICAL COMPONENTS

The electrical parts of the helicopter model are represented by two DC motors, two motor drivers, three incremental encoders, a network of resistors, and the interface board that connects these parts to the program. Aerodynamic forces move the 3-DOF system through two actuators. Two high-speed spindle bearing 750 JOHNSON 6-volt DC motors are used. A 5 mm connector is attached to the end of each motor shaft. A propeller with a pitch of 11.43 cm and a diameter of 30.48 cm is connected.

A pulse width modulation (PWM) signal controls the motor speed. BTS7960 motor drivers provide PWM signals to control motor speed. In addition, the power supply produces 12 volts and 20 amps of direct current (DC). The LM2596 DC-DC step-down regulator module protects components from high currents. Besides, the LM2596 module regulates the voltage to 12 volts and supplies 2 amps DC to incremental encoders to minimize overheating. Due to its accuracy and ability to track high-speed movements and direction in real time, the incremental encoder is often the ideal sensor for measuring the angular position of moving objects. Three Autonics incremental encoders with 4096 pulses in quadrature mode are used to measure pitch, elevation, and travel angles. The low-cost electrical circuit is shown in Fig. 3(a). Fig. 3(b), shows the

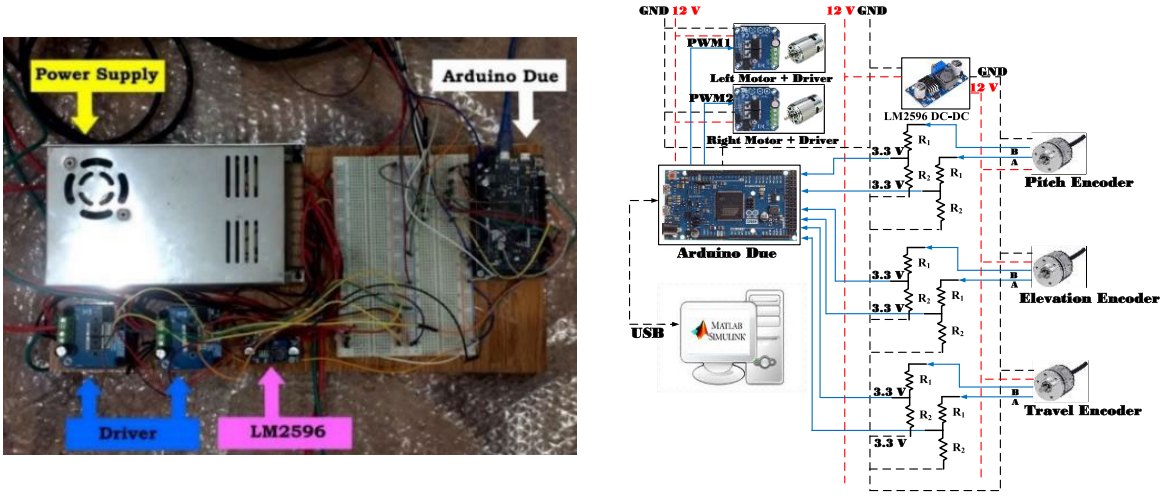

FIGURE 3. (a) Low-cost electrical setup; (b) Logic signal and power scheme for low-cost electrical setup.

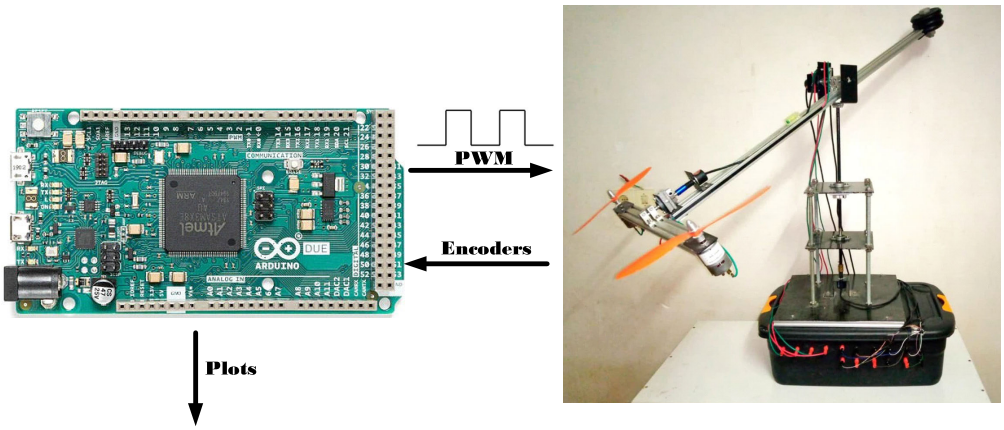

FIGURE 4. Real-time communication scheme.

logic signal and power scheme for the low-cost electrical circuit. The real-time communication scheme is presented in Fig. 4.

C. IMPLEMENTATION COST

Table 1 lists the cost of the electrical and mechanical parts for the proposed 3-DOF experimental helicopter. It is important to mention that the total cost is in line with that of a low-cost device since its assembly depends only on open-source technology. The components from Table 1 were chosen based on available components on the market and trying as much as possible to minimize the overall cost.

III. MATHEMATICAL MODEL FOR THE 3-DOF HELICOPTER

The 3-DOF helicopter is a multivariable system that can be represented by linear and nonlinear equations. The following

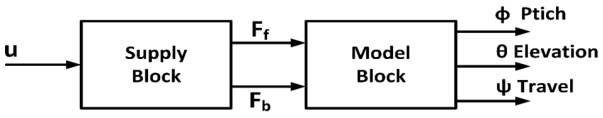

FIGURE 5. 3-DOF signals and functional blocks.

is a brief analysis of the derivation of the mathematical model.

A. ANALYTICAL MODELLING OF 3-DOF HELICOPTER

The proposed 3-DOF helicopter is considered a multivariable system containing linear and nonlinear blocks, as shown in Fig. 5.

The supply block (drivers, sensors, actuators…etc.) represents the primary electrical components. The input signal is the control signal u and the outputs are two signals fed to the model block. The first signal is F_f, and the second is

TABLE 1. Component list and cost calculation in USD.

Element Name	Element Description	Quantity	Unit price	Total price
Mechanical Components				
Main iron plate	0.4 m × 0.4 m	1	10	10
Small plate		2	5	10
Screw	0.5 m	4	5	20
Iron shaft for the travel angle	0.5 m	1	10	10
Iron shaft for the elevation angle	0.1 m	1	3	3
Iron shaft for the pitch angle	0.1 m	1	3	3
Iron brackets	0.15 m × 0.3 m	3	4	12
Coupling		3	2	6
U-shaped iron stand	0.3 m × 0.05 m	1	8	8
Long arm	1 m	1	9	9
Short arm	0.5 m	1	4.5	4.5
Electrical Components				
Arduino Due		1	42	42
Incremental Encoder	Autonics	3	94	282
Motor	750 JOHNSON, 6 V	2	8.5	17
Propeller	11.43 cm x 30.48	2	3.5	7
Power supply	12 v, 40 A	1	21	21
Motor driver	BTS7960	2	10	20
Grand Total				484.5

F_b which represents the force generated by the front motor and back motors, respectively. The model block includes all mechanical components of the system. It is also the block with the highest complexity.

B. ELECTRICAL COMPONENTS

This block relies on the transfer function of the lifting force F caused by the propellers and the number of applied voltages V. Furthermore, voltage is proportionally related to the lifting force, as presented.

$$F = kV \tag{1}$$

Remark 1: The value of constant gain k is obtained in the identification section (Section IV) experimentally.

C. MODEL BLOCK

The model block includes the mechanical parts of the 3-DOF helicopter system. Equations, including the input signals, express the analytical model of this block. The input signals are represented by F_f and F_b and the output signals are represented by ϕ, θ and ψ. The free body diagram and the orientation of the axes are described in detail in Fig. 6. The pitch motion ϕ occurs about an axis passing through the long arm of the model, and the rotation of the short arm causes this motion. In addition, the rotating elevation movement θ occurs around the horizontal Y-axis to the ground, which is the up-and-down movement of the long arm. The rotational movement of the short arm causes the travel movement ψ around the Z-axis, which is perpendicular to the ground. The thrust of the DC motor creates a revolving motion for the pitch and elevation angles and a rotational motion for the travel angle. In the same context, DC motors can be supplied with collective and differential voltages in order to have these types of movements.

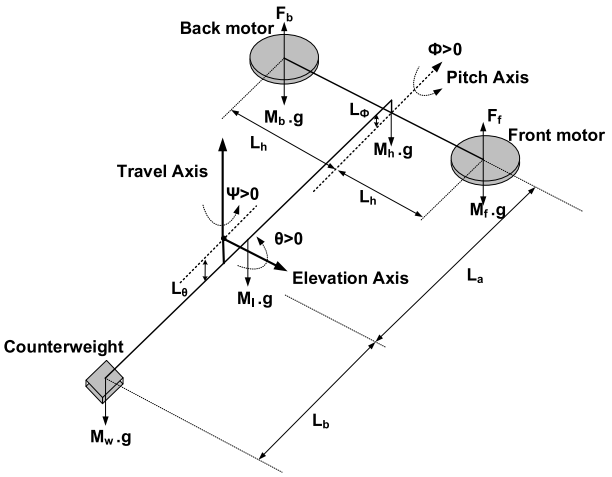

FIGURE 6. Free body diagram for the designed model.

The angles of freedom are represented by the pitch angle ϕ which is created by the revolving of the short arm around the pitch axis. The angle is considered zero when the arm is horizontal. Additionally, the elevation angle θ is generated by revolving the long arm around the global Y-axis. The angle is considered zero when the arm is in the relaxed position. Furthermore, the travel angle ψ is the angle by which the 3-DOF helicopter model is rotated around the global Z-axis. The angle is considered zero when the sensor is initialized. All angles are considered positive if the motion is

TABLE 2. Measured parameters.

Parameter	Description	value	Unit
ϕ	Pitch angle	--	Degree
θ	Elevation angle	--	Degree
ψ	Travel angle	--	Degree
L_h	Distance between the center of the propeller and the pitch axis	0.275	m
L_a	Distance between the elevation axis and the pitch axis	0.64	m
L_h	Distance between the elevation axis and the counterweight	0.45	m
L_ϕ	Distance between the pitch axis and the short arm	0.03	m
L_θ	Distance between the elevation axis and the long arm	0.03	m
L_x	Distance from the center of the long arm to the axis of rotation	0.1	m
M_f	Mass of the front rotor includes (the motor, and propeller)	0.355	kg
M_b	Mass of the back roto includes (the motor, and propeller)	0.355	kg
M_w	Mass of the counterweight	1.565	kg
M_h	Mass of the short arm	0.3678	kg
M_l	Mass of the long arm	0.68	kg
J_ϕ	Momentum of inertia on the pitch axes	0.0546	$kg.m^2$
J_θ	Momentum of inertia on the elevation axes	0.8496	$kg.m^2$
J_ψ	Momentum of inertia at travel axes.	0.8195	$kg.m^2$
g	The gravity of the earth.	9.81	$m.s^{-2}$
F_b	Force generated by the back motor	--	--
F_f	Force generated by the front motor	--	--
k_f	Force-voltage constant, (experimentally).	0.5839	$N.V^{-1}$

counterclockwise. The parameters for the helicopter are listed in Table 2.

The governing dynamic equations for the 3-DOF helicopter model are described in three angles: pitch, elevation, and travel. The mathematical model for the 3-DOF helicopter system is derived from Newton's second law as follows:

$$M = J\frac{d^2\theta}{dt^2} \tag{2}$$

where $d^2\theta/dt^2$ represents the angular acceleration in general. J_ϕ, J_θ and J_ψ denote the corresponding moment of inertia for the elevation, pitch, and travel axes, respectively. The mass-point weight M is considered to be concentrated on the motors and counterweight. Thus, the moment of inertia is calculated using the inertia definition, which takes into account the distribution of mass and its distances from the axis of rotation.

1) EQUATIONS OF MOTION

Continuing our earlier notation scheme, the rotors represented two forces acting on the system when simulating the helicopter benchmark. Pitch, elevation, and travel angles are used to obtain the governing dynamic equations [15], [38]. Considering the following assumptions below, we can establish the corresponding mathematical equations for the three angles:

Assumption 1: Due to the slow movement of the 3-DOF helicopter model compared to the real tandem helicopter, the effect of centrifugal force is assumed to be an externally bounded disturbance. However, the flight path of a conventional helicopter typically involves the helicopter experiencing the effects of centrifugal force at some point.

Assumption 2: It is assumed that the motor voltage is proportional to the thrust force [39].

Assumption 3: It is assumed that Coriolis forces acting on the propeller blades are implicitly considered in the identified dynamic equations for the propellers. However, the Coriolis effect occurs when the propeller's center of gravity shifts inward during maneuvers due to the blade flaps and deceleration motion, resulting in a reduction in the propeller's moment of inertia and a corresponding increase in its rotation velocity. Helicopters, with their huge propeller blades, are particularly susceptible to this phenomenon.

Assumption 4: Gyroscopic effects and anti-torques are canceled due to the opposite rotation of the propellers [2].

In most cases, modelling a system is based on mathematical ideas. As shown in Fig. 7(a), a system with three points (A, B, and D) experiences a rotation around point A, and two forces (at B and D) are exerted due to the presence of mass. The system experiences positive (negative) torque when F_2 (F_1) is more significant than F_1 (F_2). To model a system where the axis of rotation is not at the center of the system, four possible scenarios must be considered.

Scenario 1. As shown in Fig. 7(b), when F_2 is greater than F_1, a positive torque is experienced, causing the system to rotate counterclockwise and provide a positive pitch angle. A negative-acting torque for F_1 can be represented by the following equation:

$$T_1 = F_1 L_4 \tag{3}$$

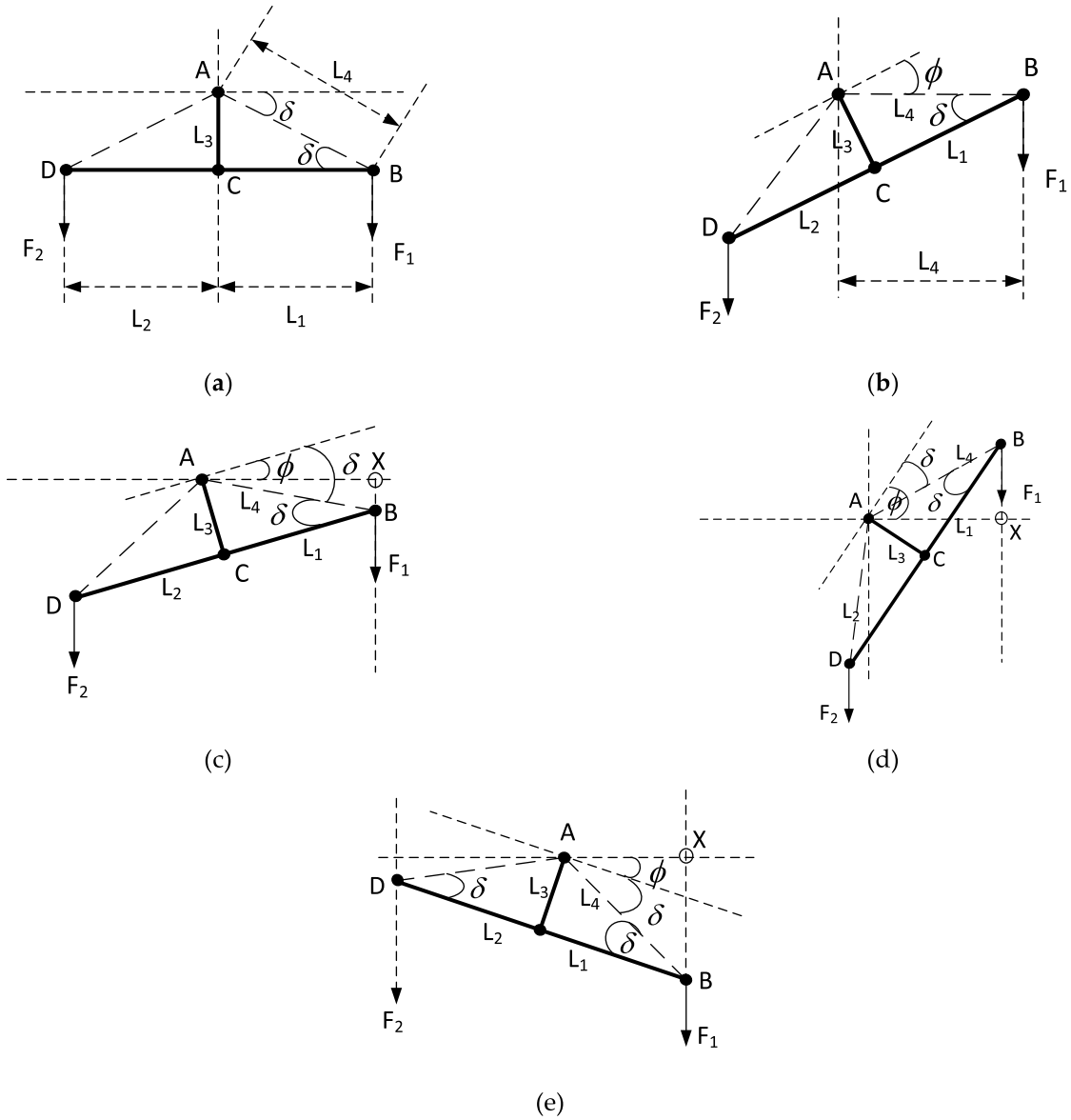

FIGURE 7. A case study of the revolved system; (a) case study; (b) scenario 1; (c) scenario 2; (d) scenario 3,(e) scenario 4.

where, L_4 is the perpendicular distance between the applied force and the axis of rotation. Therefore, the hypotenuse length L_4 can be calculated using the trigonometric formula for triangle ABC as follows:

$$L_4 = \frac{L_1}{cos\delta} \tag{4}$$

Substituting (4) into (3) yields:

$$T_1 = F_1 \frac{L_1}{cos\delta} \tag{5}$$

Scenario 2. As shown in Fig. 7(c), a positive pitch angle occurred so that from the triangle AXB, the following equation can be used:

$$\overline{AX} = cos(\phi - \delta)L_4 \tag{6}$$

Substituting (6) into (5), the negative-acting torque T_1 can be represented as follows:

$$T_1 = F_1 \frac{L_1}{cos\delta} cos(\phi - \delta) \tag{7}$$

Scenario 3. According to Fig. 7(d), a positive pitch angle occurs when the pitch angle is greater than δ angle. Obtaining (8) from the triangle AXB yields to derive (9) as follows:

$$\overline{AX} = cos(\phi - \delta)L_4 \tag{8}$$

$$T_1 = F_1 \frac{L_1}{cos\delta} cos(\phi - \delta) \tag{9}$$

Scenario 4. For the triangle AXB, when the pitch angle is less than zero, as shown in Fig. 7(e), (10) is used to derive

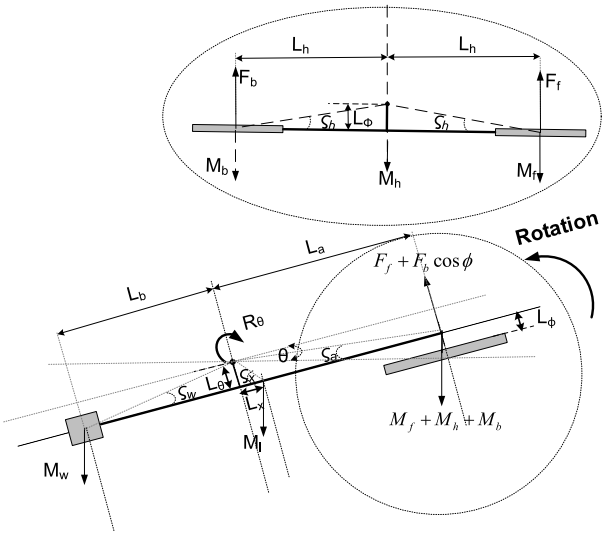

FIGURE 8. Free body diagram for elevation axis.

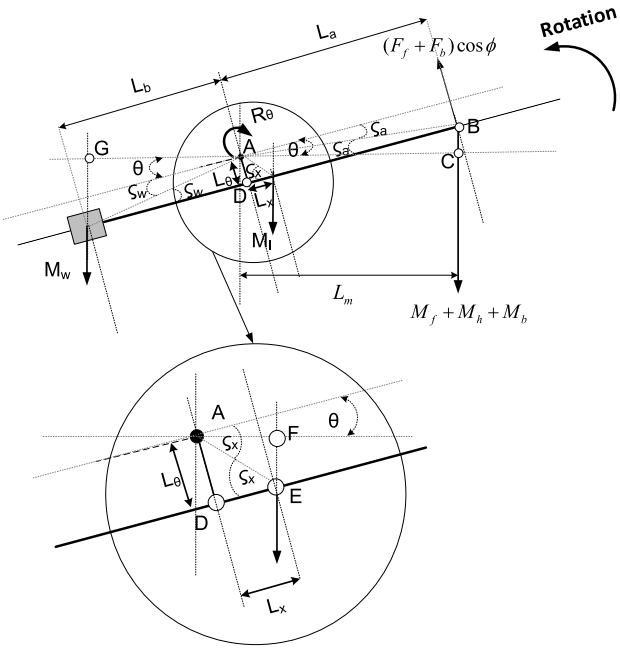

FIGURE 9. Acting torques on elevation axis.

the negative-acting torque for F_1 in (11), which satisfies the trigonometric relation for the triangles.

$$\overline{AX} = cos(\phi + \delta)L_4 \tag{10}$$

$$T_1 = F_1 \frac{L_1}{cos\delta} cos(\phi - \delta) \tag{11}$$

2) ELEVATION ANGLE

The two motors, F_f and F_b, are responsible for generating the forces that ultimately lead to the generation of the elevation momentum. As shown in Fig. 8, the long arm rotates around the elevation axis when the sum of the momentums is greater than the gravity torques. The law of conservation angular momentum expresses the differential equation that describes the movement of the elevation axis as in (2). The net torque equation is formed as follows:

$$\sum T = T_{f_\theta} + T_{b_\theta} - T_M - T_{M_l} + T_w + R_\theta + D_\theta \tag{12}$$

where T_{f_θ}, T_{b_θ}, T_M, T_{M_l} and T_w denote the torques caused by the thrust of the front motor, the thrust of the back motor, the mass of the helicopter (motors and center mass of the short arm), the center of gravity of the long arm, and the mass of the counterweight, respectively. Furthermore, D_θ is the uncertain parameter in the system. Also, $R_\theta = -f_\theta \dot{\theta}$ denotes the friction component and f_θ is the positive constant which represents the level of viscous friction in the elevation angle.

From Fig. 9, based on the previous derivation scenarios and Remark 1, the positive and negative torques are represented by the following equations:

$$\begin{cases} T_{b_\theta} = L_a F_b cos\phi \\ T_{f_\theta} = L_a F_f cos\phi \\ T_M = (M_f + M_b + M_h) g \dfrac{L_a}{cos\varsigma_a} cos(\theta - \varsigma_a) \\ T_w = M_w g \dfrac{L_b}{cos\varsigma_w} cos(\theta + \varsigma_w) \\ T_{M_l} = M_l g \dfrac{L_x}{cos\varsigma_x} cos(\theta - \varsigma_x) \end{cases} \tag{13}$$

The dynamic equation at the elevation axis is defined as:

$$\begin{aligned} J_\theta \ddot{\theta} = (F_f + F_b) cos\phi L_a - (M_f + M_b + M_h) g \frac{L_a}{cos\varsigma_a} \\ \times cos(\theta - \varsigma_a) + M_w g \frac{L_b}{cos\varsigma_w} cos(\theta + \varsigma_w) - M_l g \frac{L_x}{cos\varsigma_x} \\ \times cos(\theta - \varsigma_x) - f_\theta \dot{\theta} + D_\theta \end{aligned} \tag{14}$$

Since the propellers are rotating objects, the rotational movement of the propellers is influenced by gyroscopic precession and Coriolis forces. The 3-DOF helicopter is similar to a normal tandem helicopter, which has two engines, one at the front and one at the back, rotating in opposite directions. As a rule, aerodynamic torques, gyroscopic effects, and anti-torques cancel each other out [2]. Furthermore, the aerodynamic force can be represented using the following equation [40].

$$F = C_T \rho (\Omega R)^2 \pi R^2 \tag{15}$$

where R is the radius of the propeller blade, C_T denotes the thrust Coefficient, Ω is the frequency of rotation for the blades, and ρ is the air density. Finally, with the help of trigonometric mathematical relations, the mathematical model for the elevation angle (14) is simplified as:

$$\begin{aligned} J_\theta \ddot{\theta} = (F_f + F_b) cos\phi L_a + \big[-(M_f + M_b + M_h) g L_a + M_w g L_b \\ - M_l g L_x \big] cos\theta + \big[-(M_f + M_b + M_h) g L_a tan\varsigma_a \\ - M_w g L_b tan\varsigma_w - M_l g L_x tan\varsigma_x \big] sin\theta - f_\theta \dot{\theta} + D_\theta \end{aligned} \tag{16}$$

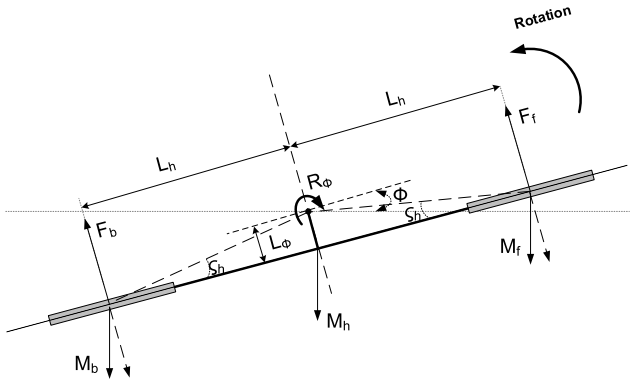

FIGURE 10. Free body diagram for Pitch axis.

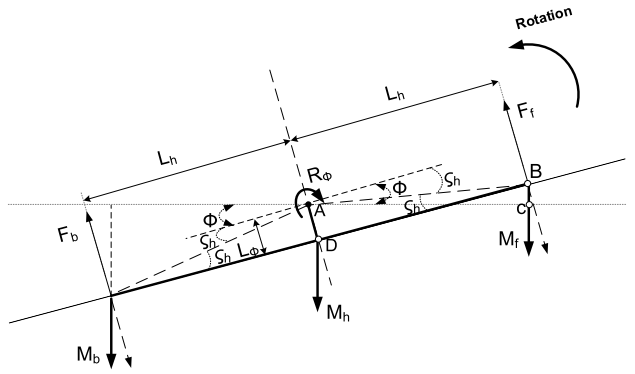

FIGURE 11. Acting torques on the pitch axis.

3) PITCH ANGLE

The pitch axis allows the short arm (helicopter) to be turned. The front and back motors' combined thrust applies torque around the pitch axis, as shown in Figs. 10 and 11.

The net torque equation is formed as follows:

$$\sum T = T_{f_\phi} - T_{b_\phi} + T_{M_b} - T_{M_h} - T_{M_f} + R_\phi + D_\phi \quad (17)$$

where, T_{f_ϕ}, T_{b_ϕ}, T_{M_f}, T_{M_b} and T_{M_h} are the torques that are caused by the thrust of the front motor, the torque that is caused by the thrust of the back motor, the torque that is caused by the mass of the front motor, the torque that is caused by the mass of the back motor and the pendulum effect torque that is caused by the center mass of the short arm, respectively. D_ϕ is the uncertain parameter in the system. Furthermore, $R_\phi = -f_\phi \dot{\phi}$ denotes the friction component and f_ϕ is the positive constant represents the viscous friction level at the elevation angle. Moreover, the following equations describe the positive and negative torques.

$$\begin{cases} T_{b_\phi} = L_h F_b \\ T_{f_\phi} = L_h F_f \\ T_{M_b} = M_b g \dfrac{L_h}{cos(\varsigma_h)} cos(\phi + \varsigma_h) \\ T_{Mf} = M_f g \dfrac{L_h}{cos(\varsigma_h)} cos(\phi - \varsigma_h) \\ T_{M_h} = M_h g L_\phi sin\phi \end{cases} \quad (18)$$

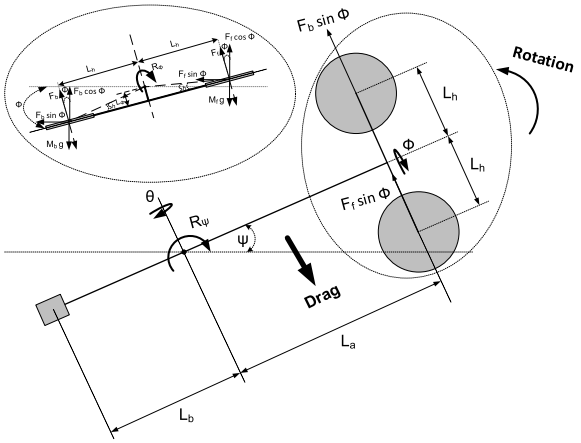

FIGURE 12. Free body diagram for travel axis.

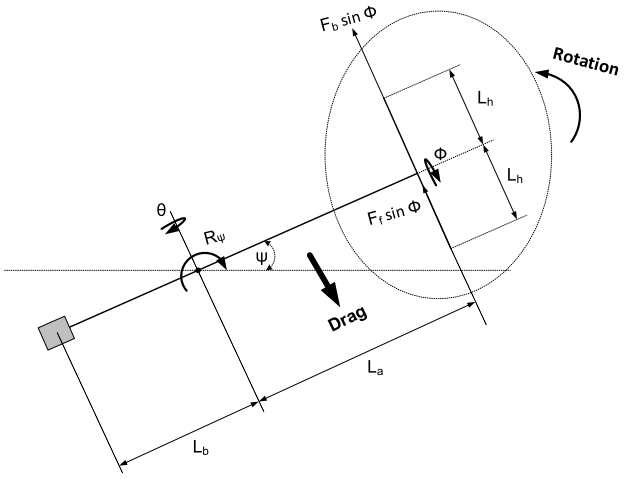

FIGURE 13. Acting torques on the travel axis.

The dynamic equation at the pitch axis is defined in (19) and simplified in (20) as follows:

$$\begin{aligned} J_\phi \ddot{\phi} = {} & (F_f - F_b)L_h + M_b g \frac{L_h}{cos(\varsigma_h)} cos(\phi + L_h) \\ & - M_f g \frac{L_h}{cos(\varsigma_h)} cos(\phi - \varsigma_h) - M_h g L_\phi sin\phi - f_\phi \dot{\phi} + D_\phi \end{aligned} \quad (19)$$

$$\begin{aligned} J_\phi \ddot{\phi} = {} & (F_f - F_b)L_h + \left[-M_f g L_h + M_b g L_h\right] cos\phi \\ & + \left[-M_b g L_h tan\varsigma_h - M_f g L_h tan\varsigma_h - M_h g L_\phi\right] sin\phi \\ & - f_\phi \dot{\phi} + D_\phi \end{aligned} \quad (20)$$

4) TRAVEL ANGLE

To adjust the travel angle, the system's long arm must be turned around the axis of motion. As shown in Fig. 12, thrust must be applied to spin the model's extended arm. The pitch angle can be adjusted finely by rotating the long arm. Fig. 13 depicts the global net torque.

The net torque equation is formed as follows:

$$\sum T = T_{f_\psi} - T_{b_\psi} + T_\phi - Drag + R_\psi + D_\psi \tag{21}$$

where, T_{f_ψ}, T_{b_ψ} and T_ϕ are the torques that are caused by the thrust of the front motor, the torque that is caused by the thrust of the back motor, and the torque that is experienced at the pitch axis, respectively. Furthermore, *Drag* is a natural phenomenon that exists due to air resistance to motion. D_ψ is the uncertain parameter in the system. Also, $R_\psi = -f_\psi \dot{\psi}$ is the friction component and f_ψ is the positive constant that represents the viscous friction level at the travel angle.

Generally, the drag experienced by a revolving body depends on its surface area. However, aerodynamic drag acts against travel motion, and the amount of resistance depends on the surface area. The following equation can be used to determine the drag in general [40]:

$$Drag = \frac{1}{2}\rho(\dot{\psi}L_a)^2 C_d A \tag{22}$$

where ρ= 1.23 kg/m^3 is the density of air, C_d is the drag coefficient, A is the cross-sectional area of the body. From Fig. 13, the positive and negative torques are represented by the following:

$$\begin{cases} T_{b_\psi} = F_b sin\phi L_a \\ T_{f_\psi} = F_f sin\phi L_a \\ T_\phi = (F_f - F_b) L_h sin\phi \\ Drag = \dfrac{1}{2}\rho(\dot{\psi}L_a)^2 C_D (A_1 + A_2 sin(\phi)) \end{cases} \tag{23}$$

The dynamic equation at the travel axis is defined as:

$$\begin{aligned} J_\psi \ddot{\psi} = {} & (F_f + F_b) sin\phi L_a + (F_f - F_b) L_h sin\phi - f_\psi \dot{\psi} + D_\psi \\ & - \frac{1}{2}\rho(\dot{\psi}L_a)^2 C_D (A_1 + A_2 sin(\phi)) \end{aligned} \tag{24}$$

where A_1 is the cross-sectional area for L_a. A_2 is the cross-sectional area for the short arm so that:

$$\begin{aligned} J_\psi \ddot{\psi} = {} & (F_f + F_b) sin\phi L_a + (F_f - F_b) L_h sin\phi - f_\psi \dot{\psi} + D_\psi \\ & - \frac{1}{2}\rho C_D A_1 (\dot{\psi}L_a)^2 - \frac{1}{2}\rho C_D A_2 (\dot{\psi}L_a)^2 sin(\phi) \end{aligned} \tag{25}$$

5) INERTIA CALCULATIONS

Based on Newton's first law of motion, inertia can be represented as:

$$I = MR^2 \tag{26}$$

where I is the inertia of an object. M, is the mass of the rotating object, and R is the radius of rotation.

As shown in Fig. 14(a), the inertia of the spinning components is determined by the axis of rotation. For the sake of clarity, the mass points in this figure are approximations made to depict the spinning masses better. However, in the physical model, there are certain minor distances between the rotating masses and the axes of rotation, and the masses' locations are set so that the Pythagoras formula is used to obtain the inertia equations for each axis. For elevation motion, the system parts rotate around the elevation axis, as shown in Fig. 14(b). The total inertia around the elevation axis is obtained as follows:

$$\begin{cases} J_\theta = \left(M_f + M_b\right)\left[(L_h^{sin\phi})^2 + L_a^2\right] + M_l\left[L_x^2 + L_\theta^2\right] \\ + M_w\left[L_b^2 + L_\theta^2\right] + M_h\left[L_a^2 + L_\theta^2\right] \\ L_h^{sin\phi} = (\sqrt{(L_\phi)^2 + (L_h)^2}) sin\phi \end{cases} \tag{27}$$

Furthermore, during the pitch motion, the short arm rotates around the pitch axis shown in Fig. 14(c), where the inertia around the pitch axis can be calculated as:

$$J_\phi = (M_f + M_b)\left[L_h^2 + L_\phi^2\right] + M_h L_\phi^2 \tag{28}$$

Besides, during travel motion, the systems' parts rotate around the travel axis, as shown in Fig. 14(d). The inertia around the travel axis can be calculated from the following formula:

$$\begin{cases} J_\theta = (M_f + M_b)\left[(L_h^{cos\phi})^2 + (L_a cos\theta)^2\right] \\ + M_l (L_x cos\theta)^2 + M_w (L_b cos\theta)^2 + M_h (L_a cos\theta)^2 \\ L_h^{cos\phi} = (\sqrt{(L_\phi)^2 + (L_h)^2}) cos\phi \end{cases} \tag{29}$$

In conclusion, the helicopter's dynamic characteristics are summed up as follows:

$$\begin{cases} \ddot{\theta} = P_1 cos\phi + P_2 cos\theta + P_3 sin\theta + P_4\dot{\theta} + P_5 + \\ P_6 cos\phi U_+ \\ \ddot{\phi} = P_7 cos\phi + P_8 sin\phi + P_9\dot{\phi} + P_{10} + P_{11} U_- \\ \ddot{\psi} = P_{12}\dot{\psi} + P_{13}\dot{\psi}^2 + P_{14} + P_{15} sin\phi + \\ P_{16}\dot{\psi}^2 sin(\phi) + P_{17} sin\phi U_+ + P_{18} sin\phi U_- \end{cases} \tag{30}$$

where, elevation dynamics parameters are as follows:

$$P_1 = \frac{-1.1678 L_a}{J_\theta},$$

$$P_2 = \frac{\left[-(M_f + M_b + M_h) g L_a + M_w g L_b - M_l g L_x\right]}{J_\theta},$$

$$P_3 = \frac{-\left[(M_f + M_b + M_h) g L_a tan\varsigma_a + M_w g L_b tan\varsigma_w + M_l g L_x tan\varsigma_x\right]}{J_\theta}$$

$$P_4 = \frac{-f_\theta}{J_\theta}, P_5 = \frac{D_\theta}{J_\theta}, P_6 = \frac{k L_a}{J_\theta}, \varsigma_a = tan^{-1}\frac{L_\theta}{L_a},$$

$$\varsigma_w = tan^{-1}\frac{L_\theta}{L_b}, \text{ and } \varsigma_x = tan^{-1}\frac{L_\theta}{L_x}$$

and, pitch dynamics parameters are:

$$P_7 = \frac{(-M_f + M_b) g L_h}{J_\phi},$$

$$P_8 = \frac{-(M_f + M_b) g L_h tan\varsigma_h - M_h g L_\phi}{J_\phi},$$

$$P_9 = \frac{-f_\phi}{J_\phi}, P_{10} = \frac{D_\phi}{J_\phi}, P_{11} = \frac{k L_h}{J_\phi}, \text{ and } \varsigma_h = tan^{-1}\frac{L_\phi}{L_h}$$

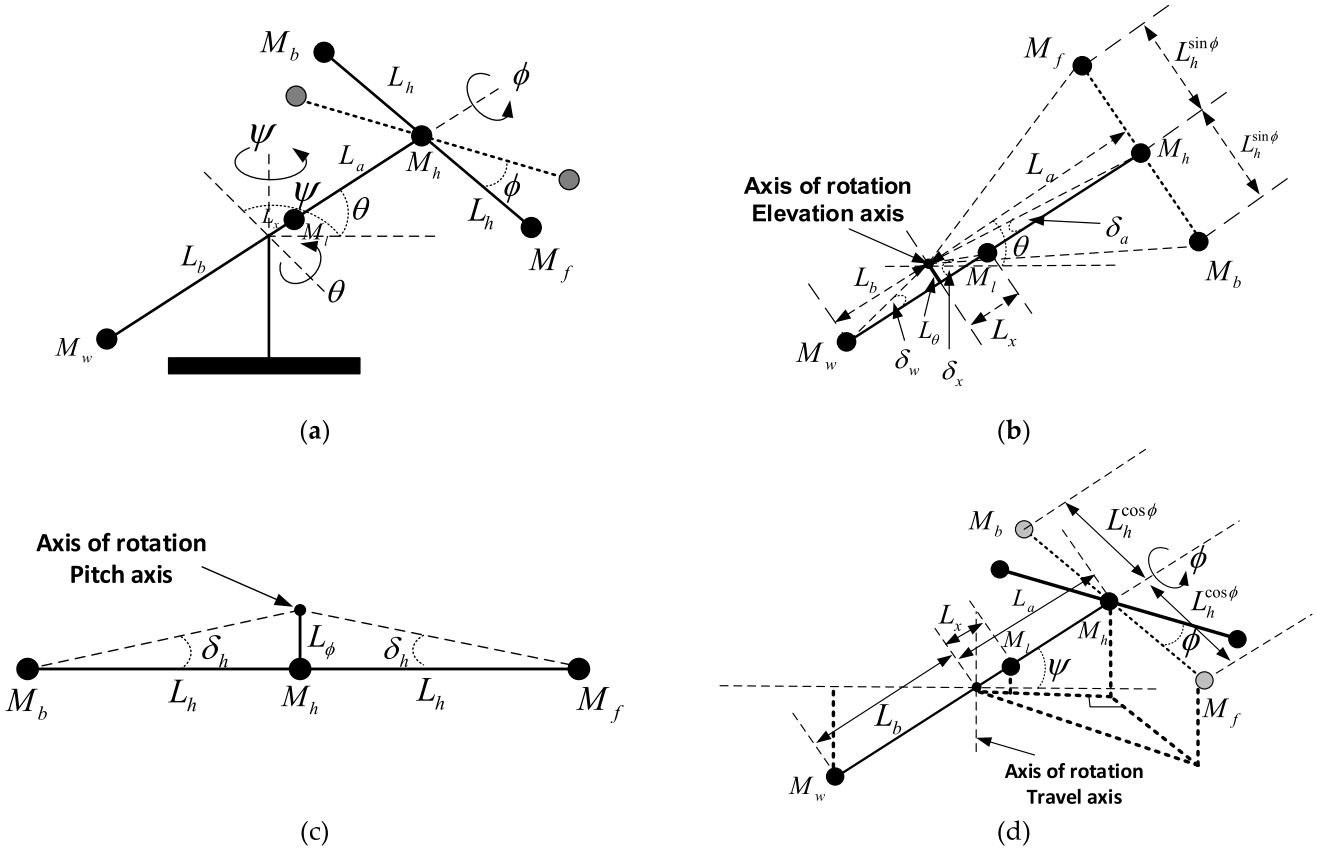

FIGURE 14. (a) Mass points representation for the model. (b) Inertia around the elevation axis. (c) Inertia around the pitch axis. (d) Inertia around the travel axis.

Also, travel dynamics parameters are as follows:

$$P_{12} = \frac{-f_\psi}{J_\psi}, P_{13} = \frac{-\rho C_D A_1 L_a^2}{2J_\psi}, P_{14} = \frac{D_\psi}{J_\psi},$$

$$P_{15} = \frac{-1.1678 L_a}{J_\psi}, P_{16} = \frac{-\rho C_D A_2 L_a^2}{2J_\psi}, P_{17} = \frac{kL_a}{J_\psi},$$

and $P_{18} = \frac{kL_h}{J_\psi}$

IV. PARAMETERS IDENTIFICATION

The mathematical model contains parameters that have been measured directly, as shown in Table 2. However, some parameters cannot be measured directly. Parameter identification procedures usually is involved in order to identify unknown parameters [41]. The following subsections are the identification procedures for the unknown parameters of dynamic equations.

A. IDENTIFICATION OF THRUST VERSUS VOLTAGES

In general, the 3-DOF helicopter is regarded as an underactuated system. It has three output signals and two input signals that control the system. The controller generates a control signal U, which affects the voltage applied to the front and the back motors. Furthermore, the speeds of the rotors and propellers will change, resulting in a change in the generated thrust. The voltage is applied to the front and back motors as a step input. The thrust force is measured, and the experimental results describe the relationship between the thrust and applied voltages for the back and front actuators using the curve fitting method presented in Fig. 15.

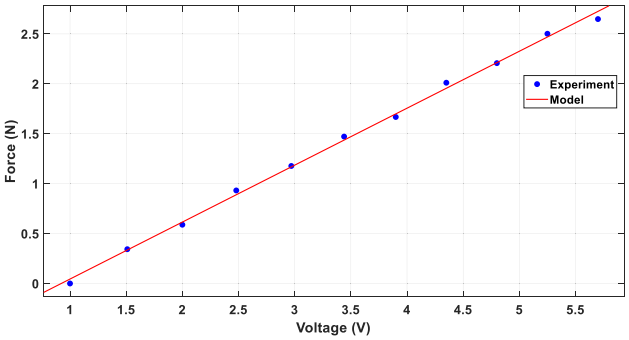

FIGURE 15. Aerodynamic force curve in terms of the control signal.

The thrust gain is obtained by curve fitting the experimental data, and the relation between the control signal and thrust for the back and front motors is obtained as:

$$F = k(V - 1) \tag{31}$$

TABLE 3. Parameter estimations for pitch axis.

Parameter	$\widehat{P}_7$	$\widehat{P}_8$	$\widehat{P}_9$	$\widehat{P}_{10}$	$\widehat{P}_{11}$
Estimated value	6.61464	-6.323	-1.395	-5.974	96.728
Tolerance	$\pm$0.1	$\pm$0.4	$\pm$0.5	$\pm$0.7	$\pm$0.5

TABLE 4. Parameter estimations for elevation axis.

Parameter	$\widehat{P}_1$	$\widehat{P}_2$	$\widehat{P}_3$	$\widehat{P}_4$	$\widehat{P}_5$	$\widehat{P}_6$
Estimated value	-56.57475	0.83576	-0.06123	-0.3366	-380.789	59.201
Tolerance	$\pm$1	$\pm$0.5	$\pm$0.1	$\pm$0.01	$\pm$5	$\pm$1

where $k \approx 0.5839$. Two types of voltages can be applied to the system, the collected and different voltages. The 3DOF helicopter is an underactuated system where the number of inputs is less than the number of outputs. Thus, the control signals for the system can be represented as:

$$\begin{cases} U_+ = V_f + V_b \\ U_- = V_f - V_b \end{cases} \tag{32}$$

B. IDENTIFICATION OF PITCH PARAMETERS

It is essential to identify the parameters for the dynamic equations to avoid high variance of the uncertainty in the design and get the highest and most reliable controller performance. Several experiments are conducted for pitch, elevation, and travel channels. First, the elevation and travel angles are physically fixed at zero to identify the pitch parameters. Two experiments are conducted by releasing the short arm from two different initial angles (13^0 and 8.8^0) and measuring the response without any prior input applied to the front and back motors, as shown in Fig. 16 (a) and (b). Then, the SSE algorithm [42], [43] is used to estimate the parameters of the pitch dynamics P_7, P_8, P_9, P_{10} and P_{11}. The values for the identified parameters are shown in Table 3.

C. IDENTIFICATION OF ELEVATION PARAMETERS

For elevation dynamics, two experiments are conducted. During these experiments, the pitch and travel angles are fixed to zero physically, and then the elevation angle is set to free. The experiments are conducted by applying step input voltages for both the front and back motors, as shown in Fig. 17 (a) and (b). Moreover, elevation dynamics parameters P_1, P_2, P_3, P_4, P_5, and P_6 are identified with specific ranges. The values of the parameters are listed in Table 4.

D. IDENTIFICATION OF TRAVEL PARAMETERS

Two experiments are conducted to identify the parameters for the travel dynamics. Step input is applied for both front and back motors with different values to accomplish different values for pitch angle during the experiments. Besides, the elevation angle is fixed to zero physically. The responses are shown in Fig. 18 (a) and (b). The identified values for the travel parameters P_{12}, P_{13}, P_{14}, P_{15}, P_{16}, P_{17} and P_{18} are listed in Table 5.

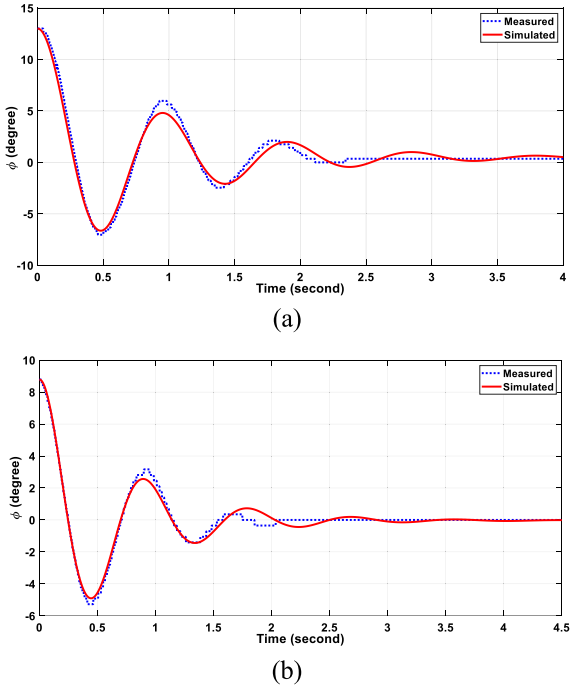

FIGURE 16. (a) Measured and simulated at pitch axis for initial angle (13^0), (b) Measured and simulated at pitch axis for initial angle (8.8^0).

The proposed model has some features concerning the counting of aerodynamic forces, friction, and drag, allowing for more accurate predictions. Also, the force-thrust constant is identified experimentally. Our sensitivity analysis for the elevation channel also demonstrated the significance of the new portions of our model. As shown in Fig. 19, we quantified the variations in system behavior when we varied the values of recent parameters in our model.

Our results show that even slight variations in parameter values can lead to large variations in system behavior. The parameters play vital role in determining the response of the system. For example, in cases 1 and 2, we noticed that slight changes in parameter values resulted in undesirable responses in practicable experiments. Furthermore, we found that neglecting certain parameters of elevation dynamics resulted in responses that were totally different from the experimental results. In addition, our model is able to

TABLE 5. Parameter estimations for travel axis.

Parameter	$\widehat{P}_{12}$	$\widehat{P}_{13}$	$\widehat{P}_{14}$	$\widehat{P}_{15}$	$\widehat{P}_{16}$	$\widehat{P}_{17}$	$\widehat{P}_{18}$
Estimated value	-0.0072	-0.0006	0.003	-0.00022	-0.224	-0.03	0.01
Tolerance	$\pm$0.01	$\pm$0.0003	$\pm$0.001	$\pm$0.0001	$\pm$0.01	$\pm$0.002	$\pm$0.001

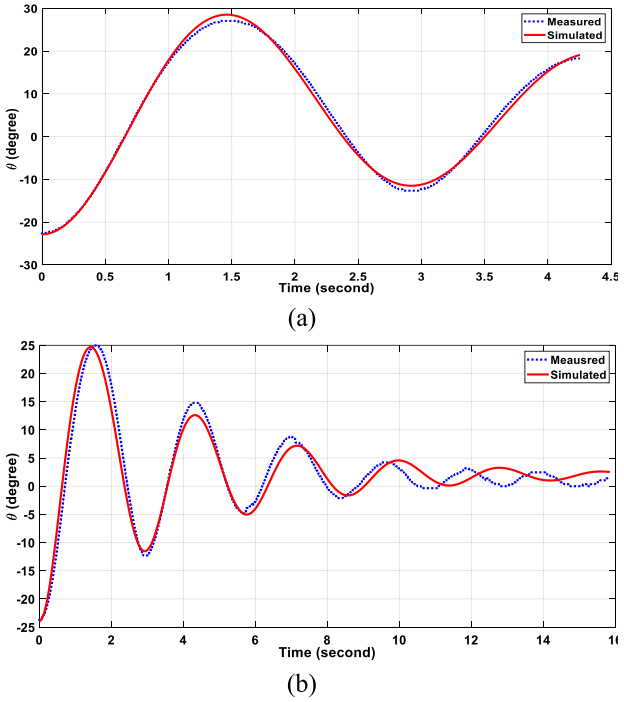

FIGURE 17. (a) Measured and simulated at elevation axis with step input 1, (b) Measured and simulated at elevation axis for step input 2.

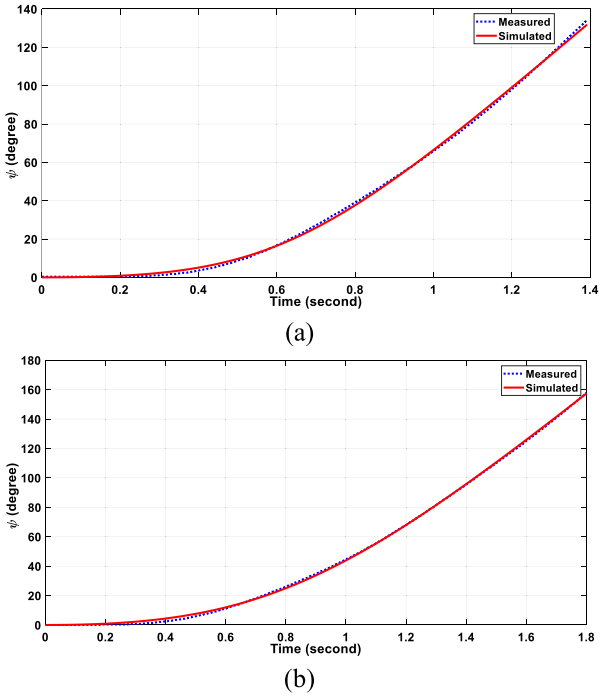

FIGURE 18. (a) Measured and simulated at travel axis for step input 1, (b) Measured and simulated at travel axis for step input 2.

provide more accurate and dependable predictions compared to existing models.

V. CONTROL SCHEME

A simple control strategy is proposed in this work since the aim is to test the usability and functionality of the proposed system. A PID controller is used because of its flexibility, robustness, and ease of implementation. Furthermore, PID control has been proven to perform satisfactorily on under-actuated systems [44], [45], which makes it a logical choice for the 3-DOF helicopter system.

The PID controller is a control strategy vastly used due to its simplicity and effectiveness in a variety of systems. PID is a non-model based method that relies on the tuning of its proportional, integral, and derivative gains to achieve the desired control objectives. Thus, the efficacy of a PID controller often hinges on how accurate the dynamics are for the controlled system. Due to this, many a time, system identification is performed even when using a PID controller.

The dynamics of our system must be carefully characterized to accomplish the precise tuning of the PID gains. System identification is the field of engineering dealing with

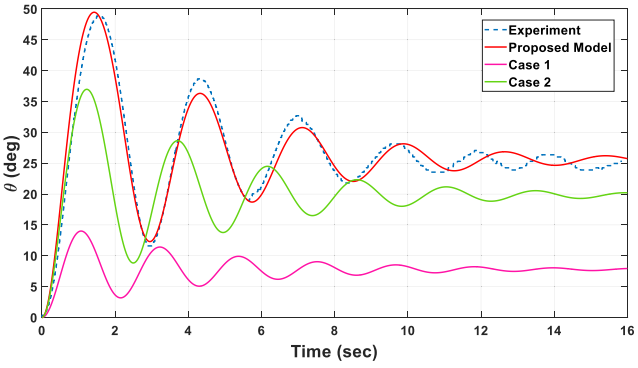

FIGURE 19. Effect of parameter variations on the elevation dynamics.

constructing mathematical models of the observed behavior of a system so that one can predict how it will respond to changes in some given inputs by understanding the system model. This predictive capability is particularly important for complex and highly interactive systems such as the 3-DOF helicopter since many separate and often nonlinear forces are operating at the same time and can sometimes interfere in counterintuitive ways.

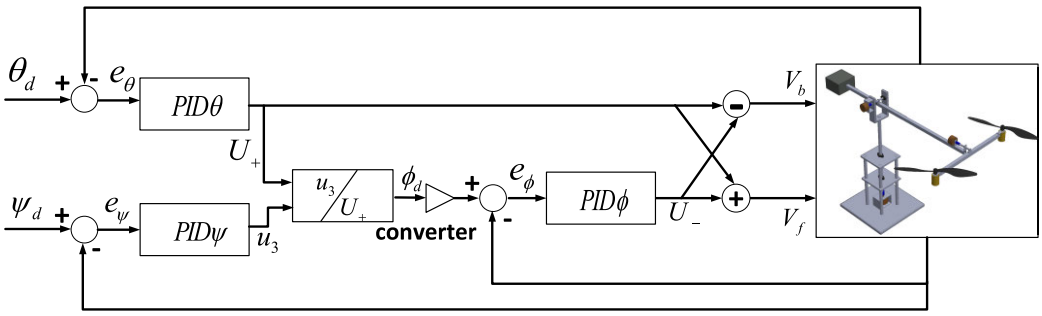

FIGURE 20. The proposed controller's scheme.

TABLE 6. Gains value.

Channel	P	I	D
Pitch	0.66	3	0.1
Elevation	0.5	1	0.1
Travel	0.13	0.7	1.462

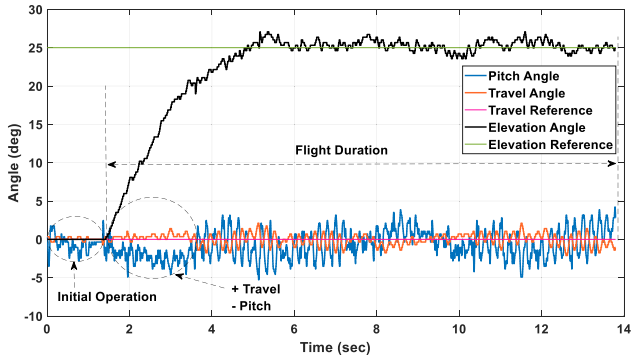

FIGURE 21. Pitch, elevation, and Travel angles during hovering mode.

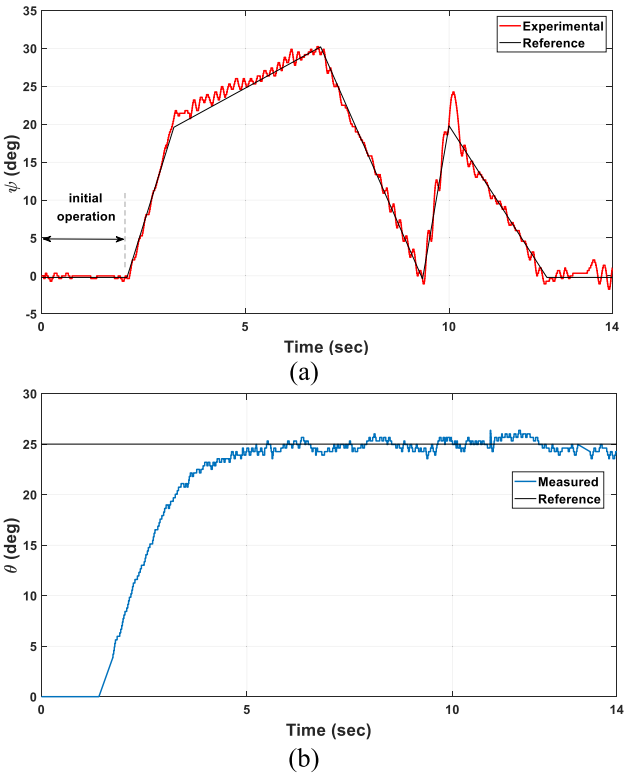

FIGURE 22. (a) Travel angle response during trajectory tracking for the irregular path, (b) Elevation angle response during flight in the irregular path.

System identification, therefore, provides insights into the system's resonant frequencies, damping ratios, and other dynamic characteristics that ultimately have a direct impact on the stability and performance of the PID controller. With a well-identified model, we can be sure that the PID controller is properly tuned to avoid instabilities and provide robust performance over a wide range of operating conditions.

The PID controllers are designed based on a cascade control concept. This concept is used to tune the controllers of multiloop control systems where nested loops exist. In the cascade control concept, the outer loop derives the set point of the inner loop, and the inner loop affects the feedback path of the outer loop. Sequentially, the closed-loop for each controller is designed for the required pairs of inputs and outputs. According to (30), it should be noted that the control performance of the travel subsystem is highly dependent on the design of the pitch subsystem. Also, the travel angle variation depends mainly on the pitch angle variation. Furthermore, travel rotation also depends on the control input U_+ as shown in (30). A virtual control signal u_3 is depicted for this purpose, presented in (33).

$$u_3 = sin\phi U_+ \tag{33}$$

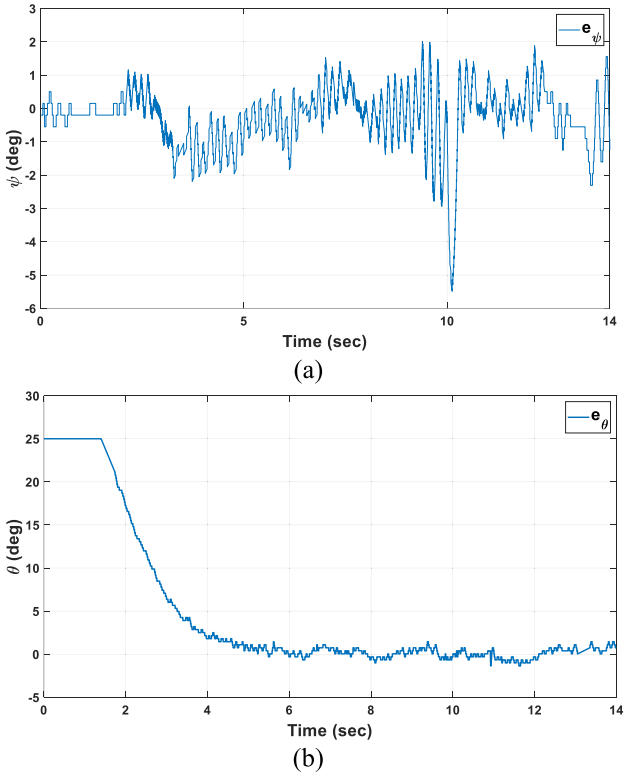

FIGURE 23. (a) Travel angle performance for the irregular path, (b) Elevation angle performance for the irregular path.

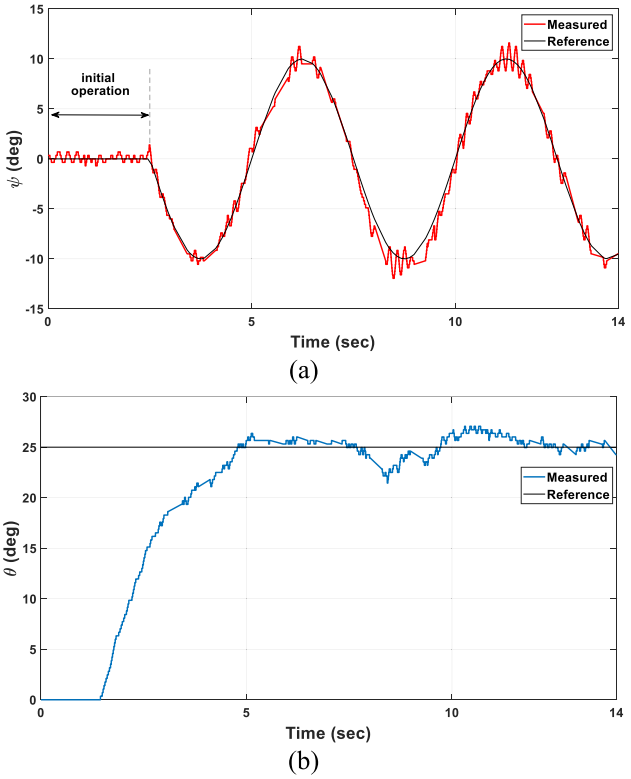

FIGURE 24. (a) Travel angle response during flight in the sinewave path, (b) Elevation angle response during the flight in the sinewave path.

The PID controllers are designed based on a mathematical model of the 3-DOF helicopter system (30). The specific equations used for the PID controllers are as follows:

$$\begin{cases} U_{-}(t) = K_{p\phi}e_{\phi}(t) + K_{i\phi}\int e_{\phi}\,(t)dt + K_{d\phi}\dot{e}_{\phi}(t) \\ U_{+}(t) = K_{p\theta}e_{\theta}(t) + K_{i\theta}\int e_{\theta}\,(t)dt + K_{d\theta}\dot{e}_{\theta}(t) \\ U_{3}(t) = K_{p\psi}e_{\psi}(t) + K_{i\psi}\int e_{\psi}\,(t)dt + K_{d\psi}\dot{e}_{\psi}(t) \end{cases} \tag{34}$$

where $U_{-}(t), U_{+}(t)$, and $U_3(t)$ are the control signals for the pitch, elevation, and travel subsystems, respectively, $e_{\phi}(t)$, $e_{\theta}(t)$, and $e_{\psi}(t)$ are the errors between the desired angle, and the measured value for each channel. $K_{p\phi}$, $K_{p\theta}$, and $K_{p\psi}$ are the proportional gain for each controller, respectively. $K_{i\phi}$, $K_{i\theta}$, and $K_{i\psi}$ are the integral gains for each controller, and $K_{d\phi}$, $K_{d\theta}$, and $K_{d\psi}$ are the derivative gains for each controller, respectively. The gains values are listed in Table 6. The control voltages V_f and V_b are applied to the front and back motors are computed from the command signals U_{+} and U_{-} as in (32). The selected closed-loop configuration is displayed in Fig. 20.

It is important to mention that it is possible to implement more intelligent control algorithms that can adapt to unknown dynamics and improve overall system performance, providing an advantage to the real nonlinear systems such as the proposed 3-DOF helicopter model. Intelligent algorithms, such as neuroadaptive control, leverage neural networks as dynamic approximators and adjust control parameters in real time. This approach is designed to handle complex underactuated systems subject to output and velocity constraints, which makes it very convenient for our model, which exhibits nonlinearity and underactuation.

Integrating these intelligent algorithms into our 3-DOF helicopter system would likely involve packaging neural network-based frameworks or adaptive controllers into our existing control architecture. This might entail training the resulting neural network with data collected from the system's responses, or it might involve designing an adaptive control scheme that can estimate the system parameters and adjust the controller accordingly. From there, we would perform a series of experiments to further refine our intelligent control algorithms.

VI. EXPERIMENTAL RESULTS

In this section, real-world experiments are conducted, including hovering and trajectory tracking scenarios. First, as an initial operation, the proposed 3-DOF helicopter required about 1.8 seconds to reach the required thrust for flight. The initial values for the three angles are 0^{o}. The most critical flight duration is when the helicopter starts to fly, which is caused by gravity drag phenomena, and it can be noticed from 1.9 to 4 seconds during the flight duration. Fig. 21 shows

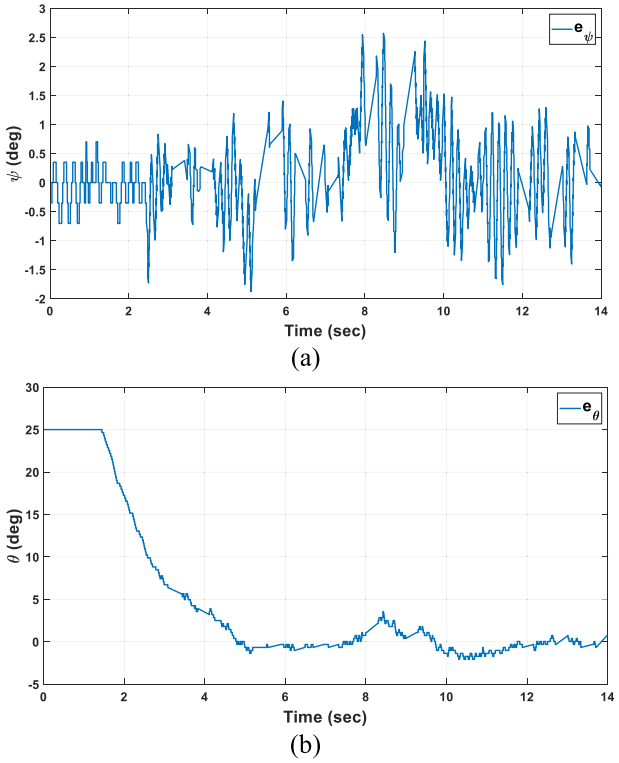

FIGURE 25. (a) Travel angle trajectory tracking performance for the sinewave path, (b) Elevation angle trajectory tracking performance for the sinewave path.

the experimental results for the desired and actual elevation, pitch, and travel angles over time during hovering mode. These experimental results show that the actual values for the elevation, pitch, and travel angles converge to the desired trajectories in minimum finite time. In addition, for trajectory tracking, two trajectories are applied in order to validate the performance of the proposed control scheme. As shown in Fig. 22(a), the results further show that the controller can compensate for errors during the flight. This can be evidenced by converging the angles to the desired values beyond a finite time. Further, the elevation response is indicated in Fig. 22(b); and the fast convergence of the angle to the target in about 3 seconds. The elevation angle remains constant in the presence of complicated interaction between the channels, reflecting the intensity of the control scheme. In addition, the trajectory tracking performances for travel and elevation angles are illustrated in Fig. 23(a) and (b), respectively. Moreover, further experiment is proposed to guarantee the performance of the control scheme, in which the sinewave trajectory is used as the input to the control system. Fig. 24 (a), and (b) represent the response of the 3-DOF helicopter throughout the flight duration. Fig. 25(a), and (b) represent the trajectory tracking performances for the sinewave path for both travel and elevation angles, respectively. Interestingly, the measured angles on the travel and elevation channels are always at minimum limits, emphasizing the exceptional capability of the control method to control multidimensional systems effectively.

VII. DISCUSSION AND LIMITATIONS

From this analysis, it can be observed that the overall procedure in a closed-loop design is relatively stable regardless of the fluctuations caused by external factors. Application of the basic conventional linear controller approach for nonlinear and unbalanced multivariate systems has been accomplished. It is also noticed that the states are never unbounded throughout the flight period. Moreover, the proposed system has certain constraints related to the low cost of the system and the high interference between channels. Overall, the system behavior is influenced by the tensile force of the cables, the interference influence of the control, the cross-coupling effect, and the wind gusts in hover and flight modes. Notably, the system is stable as it neither becomes unpredictable nor collapses into a stage of instability during the hover and flight phases. Future studies will also be undertaken to expand better control schemes for application to the 3-DOF helicopter control system.

VIII. CONCLUSION

The proposed underactuated 3-DOF experimental helicopter, which is similar to the dynamics of real tandem-rotor helicopters, has been planned and built. This paper shows the steps for constructing the helicopter, which contributes to education, and covers many topics regarding the mechanical and electrical implementation and control systems. The hardware comprises the electrical and mechanical parts, whereas the software comprises the required algorithms for data acquisition. First, the system mechanism was satisfied throughout the proposed model, and then it was modeled with the advantage of Newton's second law and SSE technique to determine system parameters. Then, for validation, the practical outcome of the implementation was compared with the simulated mathematical model using Matlab Simulink. Even though the 3-DOF helicopter system is sensitive to the environment in which it operates, the practicable result illustrates excellent stability behavior throughout hover and flight durations and furthermore the validity of the mathematical model. In addition, the robust performance of this testing rig makes it possible to adopt and verify various multivariable control schemes and identification techniques, which are of great interest in educating future professionals, notoriously, in control engineering.

ACKNOWLEDGMENT

The authors would like to thank Shahid Chamran University of Ahvaz for their financial support.

REFERENCES

[1] S. Wang, F. Jiang, B. Zhang, R. Ma, and Q. Hao, "Development of UAV-based target tracking and recognition systems," *IEEE Trans. Intell. Transp. Syst.*, vol. 21, no. 8, pp. 3409–3422, Aug. 2020.

[2] J. Fan, R. Lu, X. Yang, F. Gao, Q. Li, and J. Zeng, "Design and implementation of intelligent EOD system based on six-rotor UAV," *Drones*, vol. 5, no. 4, p. 146, Dec. 2021.

[3] K. G. Panda, S. Das, D. Sen, and W. Arif, "Design and deployment of UAV-aided post-disaster emergency network," *IEEE Access*, vol. 7, pp. 102985–102999, 2019, doi: 10.1109/ACCESS.2019.2931539.

[4] L. Yu, G. He, S. Zhao, X. Wang, and L. Shen, "Design and implementation of a hardware-in-the-loop simulation system for a tilt trirotor UAV," *J. Adv. Transp.*, vol. 2020, pp. 1–17, Oct. 2020, doi: 10.1155/2020/4305742.

[5] R. Shakeri, M. A. Al-Garadi, A. Badawy, A. Mohamed, T. Khattab, A. K. Al-Ali, K. A. Harras, and M. Guizani, "Design challenges of multi-UAV systems in cyber-physical applications: A comprehensive survey and future directions," *IEEE Commun. Surveys Tuts.*, vol. 21, no. 4, pp. 3340–3385, 4th Quart., 2019.

[6] W. Niu, B. Ning, and H. Zhou, "Design of data transmission system of human-autonomous devices for UAV inspection of transmission line status," *J. Ambient Intell. Humanized Comput.*, vol. 10, no. 9, pp. 1–10, 2019, doi: 10.1007/s12652-019-01504-x.

[7] F. Jiang, F. Pourpanah, and Q. Hao, "Design, implementation, and evaluation of a neural-network-based quadcopter UAV system," *IEEE Trans. Ind. Electron.*, vol. 67, no. 3, pp. 2076–2085, Mar. 2020, doi: 10.1109/TIE.2019.2905808.

[8] A. Boutemedjet, M. Samardžić, L. Rebhi, Z. Rajić, and T. Mouada, "UAV aerodynamic design involving genetic algorithm and artificial neural network for wing preliminary computation," *Aerosp. Sci. Technol.*, vol. 84, pp. 464–483, Jan. 2019, doi: 10.1016/j.ast.2018.09.043.

[9] M. Galimov, R. Fedorenko, and A. Klimchik, "UAV positioning mechanisms in landing stations: Classification and engineering design review," *Sensors*, vol. 20, no. 13, p. 3648, Jun. 2020, doi: 10.3390/s20133648.

[10] Y. Huang, M. Zhu, Z. Zheng, and K. H. Low, "Homography-based visual servoing for underactuated VTOL UAVs tracking a 6-DOF moving ship," *IEEE Trans. Veh. Technol.*, vol. 71, no. 3, pp. 2385–2398, Mar. 2022.

[11] H. Zhong, Y. Wang, Z. Miao, L. Li, S. Fan, and H. Zhang, "A homography-based visual servo control approach for an underactuated unmanned aerial vehicle in GPS-denied environments," *IEEE Trans. Intell. Vehicles*, vol. 8, no. 2, pp. 1119–1129, Feb. 2023.

[12] E. Gökbel, A. Güllü, and S. Ersoy, "Improvement of UAV: Design and implementation on launchability," *Aircr. Eng. Aerosp. Technol.*, vol. 95, no. 5, pp. 734–740, Mar. 2023.

[13] J. Yu, C. Peng, L. Zhang, and X. He, "Nonlinear robust attitude tracking control of 3-DOF helicopter based on output feedback," in *Proc. Int. Conf. Guid., Navigat. Control*. Singapore: Springer, 2022, pp. 5583–5594.

[14] A. L. Fradkov, B. Andrievsky, and D. Peaucelle, "Estimation and control under information constraints for LAAS helicopter benchmark," *IEEE Trans. Control Syst. Technol.*, vol. 18, no. 5, pp. 1180–1187, Sep. 2010, doi: 10.1109/TCST.2009.2033386.

[15] X. Zhu and D. Li, "Robust attitude control of a 3-DOF helicopter considering actuator saturation," *Mech. Syst. Signal Process.*, vol. 149, Feb. 2021, Art. no. 107209, doi: 10.1016/j.ymssp.2020.107209.

[16] X. Zhu and D. Li, "Robust fault estimation for a 3-DOF helicopter considering actuator saturation," *Mech. Syst. Signal Process.*, vol. 155, Jun. 2021, Art. no. 107624.

[17] Quanser. (1998). *3D Helicopter System With Active Disturbance*. Accessed: 2022. [Online]. Available: http://www.quanser.com

[18] J. Apkarian and A. Dawes, "Interactive control education with virtual presence on the web," in *Proc. Amer. Control Conf. (ACC)*, Jun. 2000, pp. 3985–3990.

[19] T. Kiefer, A. Kugi, and W. Kemmetmüller, "Modeling and flatness-based control of a 3D of helicopter laboratory experiment," *IFAC Proc. Volumes*, vol. 37, no. 13, pp. 207–212, Sep. 2004.

[20] M. Nishi, M. Ishitobi, and K. Nakasaki, "Nonlinear adaptive control system design and experiment for a 3-DOF model helicopter," *Artif. Life Robot.*, vol. 13, no. 1, pp. 50–53, Dec. 2008.

[21] A. Chabir, M. Boukhnifer, Y. Bouteraa, A. Chaibet, and J. Ghommam, "Real time fixed order robust H_∞ orientation control for 3-DOF helicopter," in *Proc. IEEE 12th Int. Multi-Conf. Syst., Signals Devices (SSD15)*, Mar. 2015, pp. 1–7.

[22] T. Kiefer, K. Graichen, and A. Kugi, "Trajectory tracking of a 3DOF laboratory helicopter under input and state constraints," *IEEE Trans. Control Syst. Technol.*, vol. 18, no. 4, pp. 944–952, Jul. 2010.

[23] F. Chen, Z. Wang, B. Jiang, and C. Wen, "An improved nonlinear model for a helicopter and its self-repairing control with multiple faults via quantum information technique," *Int. J. Control, Autom. Syst.*, vol. 13, no. 3, pp. 557–566, Jun. 2015, doi: 10.1007/s12555-013-0452-7.

[24] A. Chriette, F. Plestan, H. Castañeda, M. Pal, M. Guillo, M. Odelga, S. Rajappa, and R. Chandra, "Adaptive robust attitude control for UAVs—Design and experimental validation," *Int. J. Adapt. Control Signal Process.*, vol. 30, nos. 8–10, pp. 1478–1493, Aug. 2016.

[25] A. Chabir, M. Boukhnifer, Y. Bouteraa, A. Chaibet, and J. Ghommam, "Modelling and fixed order robust H_∞ control of aerial vehicle: Simulation and experimental results," *COMPEL Int. J. Comput. Math. Electr. Electron. Eng.*, vol. 35, no. 3, pp. 1064–1085, May 2016, doi: 10.1108/compel-06-2015-0217.

[26] S. Rajappa, A. Chriette, R. Chandra, and W. Khalil, "Modelling and dynamic identification of 3 DOF Quanser helicopter," presented at the *Proc. 16th Int. Conf. Adv. Robot. (ICAR)*, Nov. 2013, pp. 1–6.

[27] T. Zhao and W. Li, "LQR-based attitude controllers design for a 3-DOF helicopter system with comparative experimental tests," *Int. J. Dyn. Control*, vol. 12, no. 4, pp. 1063–1072, Apr. 2024.

[28] X. Wang, Z. Li, X. Yu, and Z. He, "Adaptive smooth disturbance observer-based fast finite-time attitude tracking control of a small unmanned helicopter," *J. Franklin Inst.*, vol. 359, no. 11, pp. 5322–5340, Jul. 2022, doi: 10.1016/j.jfranklin.2022.05.035.

[29] H. Peng, L. Wei, X. Zhu, W. Xu, and S. Zhang, "Aggressive maneuver oriented integrated fault-tolerant control of a 3-DOF helicopter with experimental validation," *Aerosp. Sci. Technol.*, vol. 120, Jan. 2022, Art. no. 107265, doi: 10.1016/j.ast.2021.107265.

[30] W. Xu, H. Peng, L. Yang, and X. Zhu, "Robust attitude control of a 3-DOF helicopter prototype subject to wind disturbance and communication delay," *Trans. Inst. Meas. Control*, vol. 43, no. 13, pp. 3071–3081, Sep. 2021, doi: 10.1177/01423312211021294.

[31] C. Li and X. Yang, "Neural networks-based command filtering control for a table-mount experimental helicopter," *J. Franklin Inst.*, vol. 358, no. 1, pp. 321–338, Jan. 2021, doi: 10.1016/j.jfranklin.2020.10.011.

[32] X. Yang, Y. Wang, J. Yang, and T. Wang, "Fault-tolerant control based on fixed-time observer for a 3-DOF helicopter system," *Int. J. Control, Autom. Syst.*, vol. 18, no. 12, pp. 2993–3000, Dec. 2020, doi: 10.1007/s12555-018-0849-4.

[33] X. Yang and X. Zheng, "Adaptive NN backstepping control design for a 3-DOF helicopter: Theory and experiments," *IEEE Trans. Ind. Electron.*, vol. 67, no. 5, pp. 3967–3979, May 2020, doi: 10.1109/TIE.2019.2921296.

[34] U. Pérez-Ventura, L. Fridman, E. Capello, and E. Punta, "Fault tolerant control based on continuous twisting algorithms of a 3-DoF helicopter prototype," *Control Eng. Pract.*, vol. 101, Aug. 2020, Art. no. 104486.

[35] C. K. Verginis, C. P. Bechlioulis, A. G. Soldatos, and D. Tsipianitis, "Robust trajectory tracking control for uncertain 3-DOF helicopters with prescribed performance," *IEEE/ASME Trans. Mechatronics*, vol. 27, no. 5, pp. 3559–3569, Oct. 2022, doi: 10.1109/TMECH.2021.3136046.

[36] W. Li, P. Yang, K. Geng, and X. Zhu, "Fault-tolerant attitude tracking control of tandem rotor helicopter considering internal actuator saturation and external wind gust," *Int. J. Adapt. Control Signal Process.*, vol. 37, no. 7, pp. 1671–1692, Jul. 2023, doi: 10.1002/acs.3595.

[37] A. Boubakir, S. Labiod, F. Boudjema, and F. Plestan, "Design and experimentation of a self-tuning PID control applied to the 3DOF helicopter," *Arch. Control Sci.*, vol. 23, no. 3, pp. 311–331, Sep. 2013, doi: 10.2478/acsc-2013-0019.

[38] T. Wang, M. Lu, X. Zhu, and R. J. Patton, "Aggressive maneuver oriented robust actuator fault estimation of a 3-DOF helicopter prototype considering measurement noises," *IEEE/ASME Trans. Mechatronics*, vol. 27, no. 3, pp. 1672–1682, Jun. 2022.

[39] M. Ishitobi, M. Nishi, and K. Nakasaki, "Nonlinear adaptive model following control for a 3-DOF tandem-rotor model helicopter," *Control Eng. Pract.*, vol. 18, no. 8, pp. 936–943, Aug. 2010, doi: 10.1016/j.conengprac.2010.03.017.

[40] G. Padfield, "The theory and application of flying qualities and simulation modeling," in *Helicopter Flight Dynamics* (AIAA Education Series). Washington, DC, USA: AIAA, 1996.

[41] F. Yang, Y. Li, D. Chen, S. Hu, and X. Xu, "Parameter identification of PEMFC steady-state model based on p-dimensional extremum seeking via simplex tuning optimization method," *Energy*, vol. 292, Apr. 2024, Art. no. 130601.

[42] W. Yang, Q. Du, J. Cui, Y. Wang, X. Lu, C. Qi, and G. Zhang, "Motion recognition based on sum of the squared errors distribution," *IEEE Access*, vol. 9, pp. 37116–37130, 2021.

[43] M. Bilal, S. Masud, and S. Athar, "FPGA design for statistics-inspired approximate sum-of-squared-error computation in multimedia applications," *IEEE Trans. Circuits Syst. II, Exp. Briefs*, vol. 59, no. 8, pp. 506–510, Aug. 2012.
[44] S. Zhang, X. He, H. Zhu, X. Li, and X. Liu, "PID-like coupling control of underactuated overhead cranes with input constraints," *Mech. Syst. Signal Process.*, vol. 178, Oct. 2022, Art. no. 109274.
[45] J. G. Romero, A. Donaire, R. Ortega, and P. Borja, "Global stabilisation of underactuated mechanical systems via PID passivity-based control," *Automatica*, vol. 96, pp. 178–185, Oct. 2018.

OSAMAH TALAL MAKKI received the B.Sc. degree in control engineering from the Control and Systems Engineering Department, University of Technology, Baghdad, Iraq, in 2004, and the M.Sc. degree in advance control and real-time systems from the Department of Automatic Control and System Engineering, Politehnica University of Bucharest, Bucharest, Romania, in 2017. He is currently pursuing the Ph.D. degree with the Faculty of Engineering, Shahid Chamran University of Ahvaz, Ahvaz, Iran. He is a Lecturer and a Researcher with the Faculty of Engineering, University of Kerbala, Karbala, Iraq. His areas of research interests include advanced control, nonlinear control, real-time systems, and systems engineering.

SEYYED SAJJAD MOOSAPOUR received the B.Sc. degree in control engineering from the Sahand University of Technology, Tabriz, Iran, in 2003, and the M.Sc. and Ph.D. degrees in control engineering from the University of Tabriz, Tabriz, in 2006 and 2012, respectively. He is currently an Associate Professor with the Shahid Chamran University of Ahvaz, Ahvaz, Iran. His areas of research interests include nonlinear control, sliding mode control, and disturbance observer.

SALEH MOBAYEN (Member, IEEE) received the B.Sc. and M.Sc. degrees in control engineering from the University of Tabriz, Tabriz, Iran, in 2007 and 2009, respectively, and the Ph.D. degree in control engineering from Tarbiat Modares University, Tehran, Iran, in January 2013. From February 2013 to December 2018, he was an Assistant Professor and a Faculty Member with the Department of Electrical Engineering, University of Zanjan, Zanjan, Iran. Since December 2018, he has been an Associate Professor of control engineering with the Department of Electrical Engineering, University of Zanjan. He currently collaborates with the National Yunlin University of Science and Technology as an Associate Professor with the Future Technology Research Center. He has published several articles in the national and international journals. His research interests include control theory, sliding mode control, robust tracking, non-holonomic robots, and chaotic systems. He is a member of the IEEE Control Systems Society and program committee of several international conferences. He is an Associate Editor of *Artificial Intelligence Review*, *International Journal of Control, Automation and Systems*, *Circuits, Systems, and Signal Processing*, *Journal of Simulation*, *Measurement and Control*, *Complexity*, *International Journal of Dynamics and Control*, *SN Applied Sciences*, and other international journals, and an Academic Editor of *Mathematical Problems in Engineering*.

JAFAR HEYRANI NOBARI received the B.Sc. degree in electrical engineering from the Sharif University of Technology, in 1990, the degree from TU Delft, and the Ph.D. degree in electrical engineering in the trend of control from Tarbiat Modares University, in 2000. He is currently an Assistant Professor with the Department of Systems and Control, Faculty of Electrical Engineering, K. N. Toosi University of Technology. His research interests include navigation, flight and guidance control, and digital and nonlinear control.